Applied Catalysis B: Environmental 235 (2018) 238–245

Contents lists available at ScienceDirect

Applied Catalysis B: Environmental

journal homepage: www.elsevier.com/locate/apcatb

# CuI-BiOI/Cu film for enhanced photo-induced charge separation and visible-light antibacterial activity

Yiqiu Zhang[a], Chen Lin[a], Qun Lin[c], Yubo Jin[a], Yonghao Wang[b,*], Zizhong Zhang[a], Huaxiang Lin[a,*], Jinlin Long[a], Xuxu Wang[a]

[a] College of chemistry of Fuzhou University, State Key Laboratory of Photocatalysis on Energy and Environment, Fuzhou University, Fuzhou, 350116, China
[b] College of Environment and Resources, Fuzhou University, Fuzhou 350108, China
[c] Department of Anesthesia, The First Affiliated Hospital, Fujian Medical University, Fuzhou, 350002, China

ARTICLE INFO

*Keywords:*
CuI-BiOI/Cu film
Photocatalysis
Disinfection
Charge separation

ABSTRACT

CuI-BiOI/Cu film with effective photocatalytic inactivation of E. coli under visible-light-driven (VLD) were prepared on copper sheet and were characterized by TEM, SEM, XRD, XPS and DRS. The photocatalytic inactivation of E. coli of CuI, BiOI, CuI-BiOI and CuI-BiOI/Cu film were investigated. The results showed that CuI-BiOI/Cu film exhibit the most excellent bacteria disinfection activity, and the quantity of viable bacteria could almost inactivate after being illuminated for 2 h. The Laser Scanning Confocal Microscopy (LSCM) observation exhibits that the morphology of bacteria changed a lot after visible light irradiation, and the UV spectra confirm the leakage of bacterial protein. The antibacterial mechanism was studied by employing photoelectrochemical techniques and scavengers of different reactive species, which reveals that the effect of reactive species on the antibacterial activity decrease in order $h^+ > e^- > H_2O_2 > \cdot HO > \cdot O_2^-$. The CuI and Cu play the important role in the separation of $h^+$ and $e^-$. During the photocatalytic process, the CuI act as a hole-transport channel and the Cu act as electron transfer for CuI-BiOI heterostructure, which promotes the separation of photo-generated charges and enhances the photocatalytic antibacterial activity of the as-prepared samples.

## 1. Introduction

Water is an essential element for human daily life. However, microbial contamination in water has been a constant threat to human health all over the world. Millions of people die of diseases and disabilities caused by pathogenic microorganisms each year [1,2]. Hence, rapid and efficient disinfection methods for drinking water are urgently required. However, traditional water treatment technology, such as UV disinfection, chlorination and filtration techniques, unavoidably append noxious disinfection by products (DBPs). Solar energy is an attractive renewable-energy resource and can be used for water disinfection via the solar disinfection of drinking water. Recently, photocatalytic disinfection, an economical, effective and environmentally friendly photooxidation process, has attracted more and more attention from the perspective of using abundant solar energy and low toxicity [3–5].

Bismuth oxyhalides BiOX (X = Cl, Br, I), a category of Bi-based semiconductors with outstanding optical and electrical properties, have exhibited great potential in water disinfection and attractive photocatalytic activity on the degradation of organic pollutant because of its low toxicity, chemical stability, and inexpensiveness [6–12]. BiOI is one of the most suitable visible light photocatalyst due to its narrow band gap (1.8 eV), which enables it to be applied in treatment of Microorganisms in water under visible light. However, the small band–gap leads to the high recombination efficiency of photo-generated $e^-$-$h^+$ pairs that limits its photocatalytic disinfection efficiency. In general, the photocatalytic disinfection efficiency mainly relies on the $e^-$ which can directly attract bacterial and on oxygen species (ROS) such as $\cdot O^{2-}$ and $\cdot OH$ that were generated by photo-exited electron and hole, respectively [3]. In fact, most of the photo-excited electrons and holes rapidly recombine and only few of them can transfer to photocatalyst surface and participate in the disinfection process. Hence, to many efforts, including the fabrication of heterojunction structure orfabrication of heterojunction structure or developing modified BiOI, have been conducted to suppress the recombination of photogenerated electron–hole pairs of BiOI, and then enhance their visible light driven (VLD) [11].

The Cuprous iodide (CuI), a P-type semiconductor material, which steadily exists as γ crystalline phase when temperatures below 350 °C, has attracted great attention due to its particular features, especially its active layers for hole transportation. Some studies have reported that

* Corresponding authors.
*E-mail addresses:* wangyh@fzu.edu.cn (Y. Wang), lhx@fzu.edu.cn (H. Lin).

https://doi.org/10.1016/j.apcatb.2018.05.001
Received 2 February 2018; Received in revised form 16 April 2018; Accepted 2 May 2018
Available online 02 May 2018

CuI exhibit high mobility of hole and improve the photoelectrocatalytic activity of CuI-BiOI heterojunction [13]. If the fascinating optical properties of BiOI combined with CuI, the CuI could be used as a hole-transport channel for CuI-BiOI heterostructure and charger separation might be improved. Hence, in this work, we prepared CuI-BiOI on copper sheet by water bath method. The photocatalytic antibacterial activity and stability of CuI-BiOI/Cu film were assessed by using E. coli K – 12 as model bacterium. To compare, the antibacterial activity of BiOI, CuI and CuI-BiOI were investigated under the same condition. By further detecting the generation of reactive oxygen species (ROS), the reasonable mechanism of photocatalytic antibacterial activity of CuI-BiOI/Cu film was discussed. It is hoped that our work offered a possibility to achieve more efficient water disinfection method.

## 2. Experimental

### 2.1. Materials

The copper sheets were purchased by Tianjin Fuchen Chemical Reagents Factory, bismuth nitrate pentahydrate ($Bi(NO_3)_3{\cdot}5H_2O$, AR), potassium iodide (KI, AR), silver nitrate ($AgNO_3$, AR), ethylene glycol (AR), Polyvinyl Pyrrolidone (PVP, AR), Polyethylene Glycol (PEG, AR), Hydroiodic Acid (HI, AR) were purchased from Sinopharm Chemical Reagent Co., Ltd., China without any further purification, the human serum albumin (HSA) was purchased by CSL Behring L.L.C., U.S.A. The bacterial cells were cultured in ueller hinton broth solution at 37 °C for 18 h and immediately diluted. The concentration of cell density is $10^{6.5}$ cfu (colony forming unit)/ml. Deionized water was also used in all the experiments. All glass apparatuses used were washed with deionized water, and then autoclaved at 121 °C for 20 min.

### 2.2. Synthesis of BiOI

4 mmol $Bi(NO_3)_3{\cdot}5H_2O$ was added into 40 ml of mixture solution of EG/water (the volume ratio of EG to water was maintained at 7:1) containing 4 mmol KI with 50 mg PVP. After stirring for 2 h, the mixture solution was transferred into a 100 ml Teflon–lined stainless autoclave. The autoclave was heated at 140 °C for 4 h under autogenous pressure, and then it was cooled to room temperature naturally. The resulting products of BiOI were gathered and rinsed with deionized water and ethyl alcohol thoroughly, and finally dried at 60 °C.

### 2.3. Fabrication of CuI-BiOI film on copper sheet

The copper sheets were first cleaned with acetone and ethanol, and water subsequently. Afterward, the cleaned copper sheets were immersed in 0.1 M HCl solution for 15 min to clear the surface oxidization layer and then were dried at 60 °C. Then the obtained BiOI sample was added into 50 ml solution containing 10 g PEG. The treated copper sheets with a lateral size of 35 mm × 35 mm were immersed in mixture solution immediately. After stirring in a 70 °C water bath for 24 h, then the obtained CuI-BiOI/Cu film were dried at 60 °C overnight.

### 2.4. Characterization

Crystal structure identification was performed using Bruker D8 X–ray diffractometer (XRD) with Cu Kα radiation operating at 40 kV and 40 mA. The morphologies of CuI-BiOI were observed by a scanning electron microscopy (SEM, ZEISS SUPRA 55), transmission electron microscopy (TEM, Tecnai F20) and elemental mapping patterns were investigated using OXFORD EDX 6767. The morphology of bacteria was observed by a Laser Scanning Confocal Microscopy (LSCM, Leica DMI4000 CS) Diffuse reflection spectra (DRS) of the samples were recorded on a Varian Cary–500 spectrophotometer, using $BaSO_4$ as the reference. The X-ray photoelectron spectroscopy (XPS) measurements of the samples were carried out on a ESCALAB 250 photoelectron spectrometer (Thermo Fisher Scientific) at $3.0 \times 10^{-10}$ mbar with monochromatic Al Kα radiation (E = 1486.2 eV). UV–vis spectroscopy (Shimadzu, UV-1780) was used to detect the leakage of bacterial cell contents. Photoelectrochemical characterization was conducted on a ZENNIUM electrochemical workstation (Zahner, Germany) with a standard three-electrode system. The prepared samples served as the working electrode with an active area of ca. 0.25 $cm^2$. The counter and reference electrodes were Pt plate and Ag/AgCl electrode and 0.2 M $Na_2SO_4$ (pH = 6.8) was used as electrolyte. The electrochemical impedance spectroscopy (EIS) measurement was measured *via* an EIS spectrometer (CHI-660D workstation, CH Instrument) in the three-electrode cell in the presence of 0.5 M KCl solution containing 5.0 mM $K_3[Fe(CN)_6]/K_4[Fe(CN)_6]$ by applying an AC voltage with 5 mV amplitude in a frequency range from 1 Hz to 100 kHz under open circuit potential conditions. The cyclic voltammograms (CV) were measured in the same solution in the three electrode cell as that of the EIS measurement on the BAS Epsilon workstation. The cathodic polarization curves were obtained using the linear sweep voltammetry (LSV) technique with a scan rate of 5 mV $s^{-1}$.

### 2.5. Photocatalytic disinfection performance

*E. coli* K – 12 was used as a model bacterium to investigate the antimicrobial activity of CuI film and CuI-BiOI. The bacterial cells were cultured in nutrient broth at 37 °C. During each test, 40 ml bacterial PBS solution ($1 \times 10^{6.5}$ cfu/ml) was poured into a pyrex glass reactor which contained a 1 cm × 1 cm CuI or CuI-BiOI. These *E. coli* solutions were then irradiated with a Xe lamp equipped with a long–pass cut–off filter VL (300 W, $\lambda \geq 400$ nm). Aliquots (0.5 ml) of photo-treated *E. coli* solutions were withdrawn at regular time intervals, diluted and spread on freshly prepared agar plates and incubated at 37 °C for 24 h.

### 2.6. Laser scanning confocal microscopy (LSCM) observation of bacteria

Bacterial LSCM was used to visualize the changes of cell morphologies. The phototreated bacteria at different irradiation time intervals (0, 1 and 2 h) were uniformly dispersed on the glass bottom cell culture dishes for LSCM.

### 2.7. The UV absorption of the bacterial protein

The UV absorption was used to confirm the leakage of the bacterial protein after visible light irradiation. Then the photo-treated bacteria at different irradiation time intervals (0, 1 and 2 h) were diluted with PBS solution, the prepared bacterial fluid was used for UV test.

## 3. Results and discussion

### 3.1. Properties of CuI-BiOI

Fig. 1 shows X–ray diffraction (XRD) images of CuI-BiOI, pure BiOI and CuI in the range of $15° < 2\theta < 80°$. The BiOI peaks appeared at 24.3° (101), 29.7° (102), 31.7° (110) and 49.9° (005) which could be well-indexed to the standard tetragonal phase of BiOI (JCPDS Card No.10–0445). The typical diffraction peaks of CuI appeared at 25.5° (111), 42.2° (220) and 49.9° (311), which could be attributed to γ crystalline phase of CuI (JCPDS Card No. 06–0246). In addition, two sets of diffraction peaks of BiOI and CuI can be seen in the XRD patterns of CuI-BiOI indicating that CuI-BiOI have high crystallinity. However, the XRD peaks corresponding to BiOI in the patterns of CuI-BiOI became weaker and broader than that of pure BiOI, suggesting that the growth of BiOI has been suppressed by CuI in the preparing process.

The typical SEM and TEM images of CuI-BiOI were shown in Fig. 2. As can be seen from Fig. 2a, CuI-BiOI exhibits flower-like network hierarchical microstructures, which are assembled by a large number of BiOI nanosheets and irregular CuI particles. As shown in Fig. 2c, the

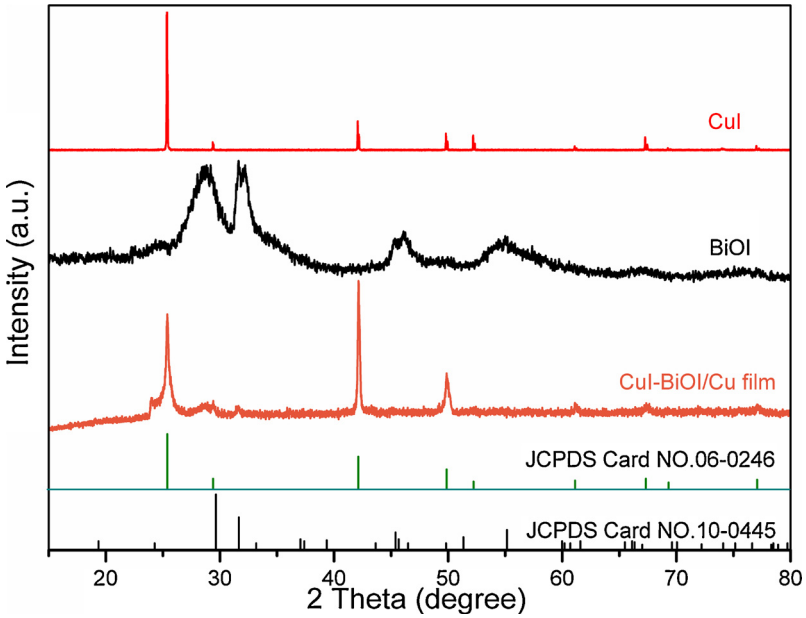


**Fig. 1.** XRD patterns of BiOI, CuI and CuI-BiOI.

lattice fringes of BiOI and CuI were 0.31 and 0.21 nm, which were in accordance with the interplanar spacing of (1 0 2) plane and (2 2 0) plane of BiOI and CuI, respectively, indicating that CuI-BiOI sample was highly crystalline. Fig. 2d was a representative image of CuI-BiOI with a corresponding energy–dispersive X–ray spectroscopy (EDS) elemental mapping for Bi (Fig. 2e), O (Fig. 2f), Cu (Fig. 2g), and I (Fig. 2h). In this elemental map, the brighter area indicated a higher concentration of the corresponding element. Obviously, the elements of Bi, O, I, and Cu were well–dispersed in the CuI-BiOI, confirming the successful synthesis of CuI-BiOI.

XPS spectra were carried out to further analyze the chemical composition and chemical states of the CuI-BiOI. As can be seen from the survey spectra of CuI-BiOI (Fig. 3a), the CuI-BiOI consists of Bi, O, I and Cu elements, which is well in accordance with the EDS results. Fig. 3b reveals the high-resolution spectra for the Bi 4f with two peaks at 164.4 eV and 159.2 eV, suggesting that the existence of $Bi^{3+}$ [18,19] in the CuI-BiOI. As shown in fig. 3c, two contributions are observed at 934.6 eV and 932.6 eV. The higher BE peak at ~935 eV is assigned to $Cu^{2+}$, accompanied by the characteristic $Cu^{2+}$ shakeup satellite peaks (938 – 945 eV). The lower BE peak at ~932 eV suggests the presence of $Cu^{+}$ or Cu° species. In general, it is difficult for Cu $2p_{3/2}$ XPS to differentiate between $Cu^{+}$ and Cu°. In addition, Auger Cu LMM spectra are often used to confirm the presence of $Cu^{+}$ at BE ~570 eV [20,21]. In this sample, an obvious Cu LMM spectra with peak at 570 eV indicated that the lower BE peak at ~932 eV is ascribed to $Cu^{+}$ (insert in Fig. 3c). Moreover, the two individual peaks of Cu $2p_{1/2}$ and $2p_{3/2}$ at 952.4 eV and 932.6 eV, with a peak separation of 19.8 eV, implies the presence of $Cu^{+}$ [14–17]. The $I3d_{5/2}$ peaks for the CuI-BiOI can be deconvoluted into two peaks at 618.8 eV and 619.8 eV. The peaks at 618.8 eV ($I3d_{5/2}$) and 630.1 eV ($I3d_{3/2}$) are assigned to $I^{-}$ in BiOI [22,23], and the peaks at 619.8 eV ($I3d_{5/2}$) and 631.4 eV ($I3d_{3/2}$) are assigned to $I^{-}$ in CuI [14,15]. All of the above results confirm that the coexistence of BiOI and CuI in CuI-BiOI.

The optical properties of the samples were analyzed by UV–vis diffuse spectra. As shown in Fig.4, the adsorption edge of pure CuI and pure BiOI are about at 420 and 641 nm that are similar to that reported by reference [13], respectively. However, when compared to CuI and BiOI, the CuI-BiOI showed obvious red-shift absorption with the

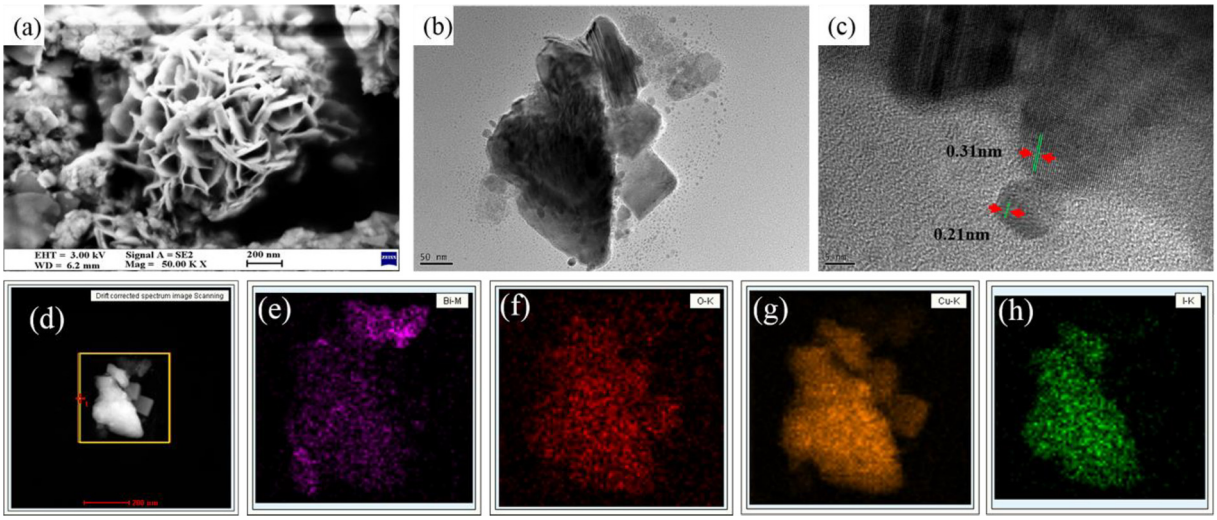


**Fig. 2.** SEM images of CuI-BiOI (a), TEM of CuI-BiOI (b), HRTEM image of CuI-BiOI (c) and corresponding energy–dispersive X–ray spectroscopy (EDS) elemental mapping for Bi (e), O (f), Cu (g) and I (h).

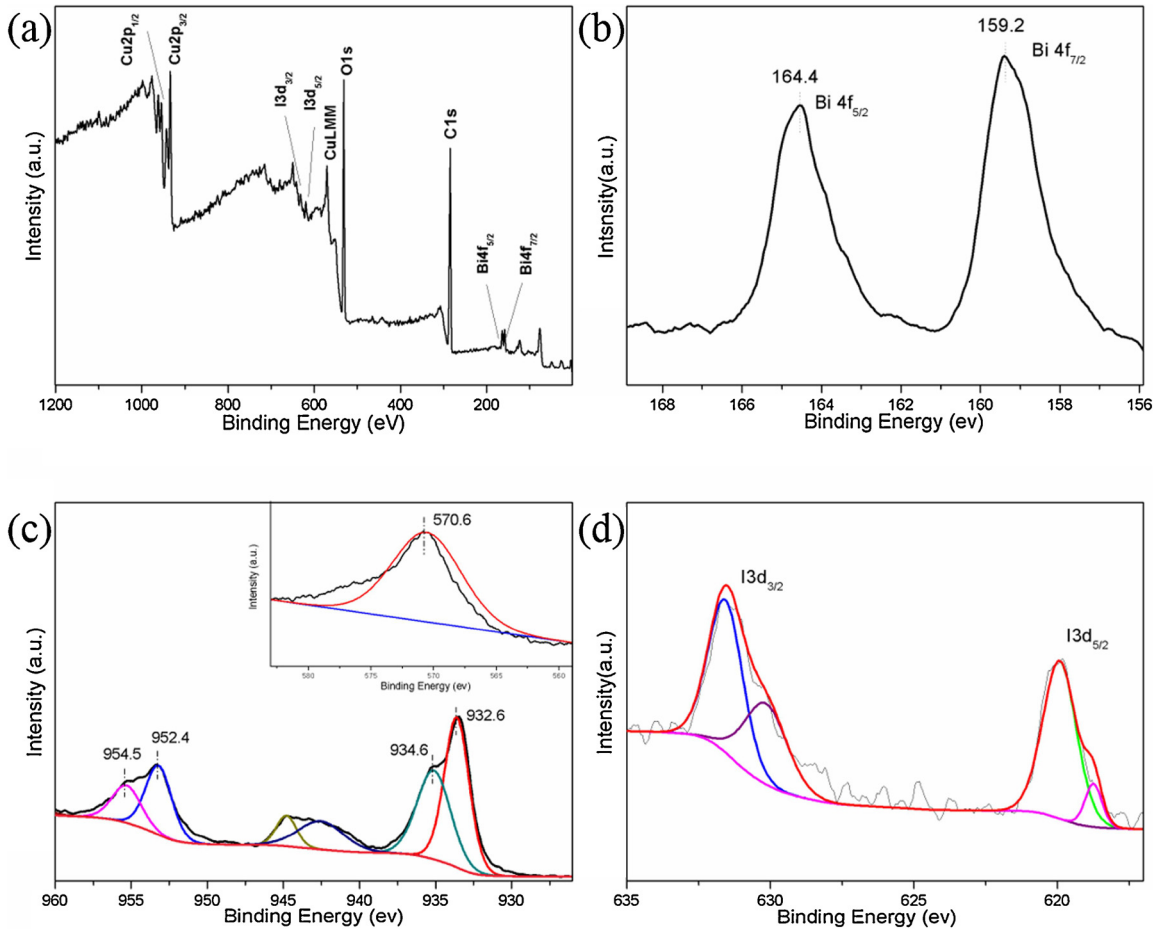


**Fig. 3.** High–resolution XPS spectra: (a) overall XPS spectra of CuI-BiOI, (b) Bi 4f of CuI-BiOI, (c) Cu 2p of CuI-BiOI, and (d) I 3d of CuI-BiOI.

absorption edge is up to 697 nm, which indicates that CuI-BiOI can absorb much more visible light in the solar spectrum.

### 3.2. Photocatalytic disinfection performance

The photocatalytic disinfection activity of prepared samples was assessed by the inactivation of *E. coli* for different time intervals (0, 0.5, 1, 1.5, and 2 h) in the mixed suspension of *E. coli* ($10^{6.5}$ cfu/mL) under VL. As can be seen in Fig. 5a, all of the catalysts showed negligible disinfection efficiencies in dark. In Fig. 5b, both pure BiOI and CuI powders displayed less cytotoxicity to *E. coli* under visible light, and the quantity of viable bacteria reduced to $10^{5.5}$ and $10^{4.8}$, respectively.

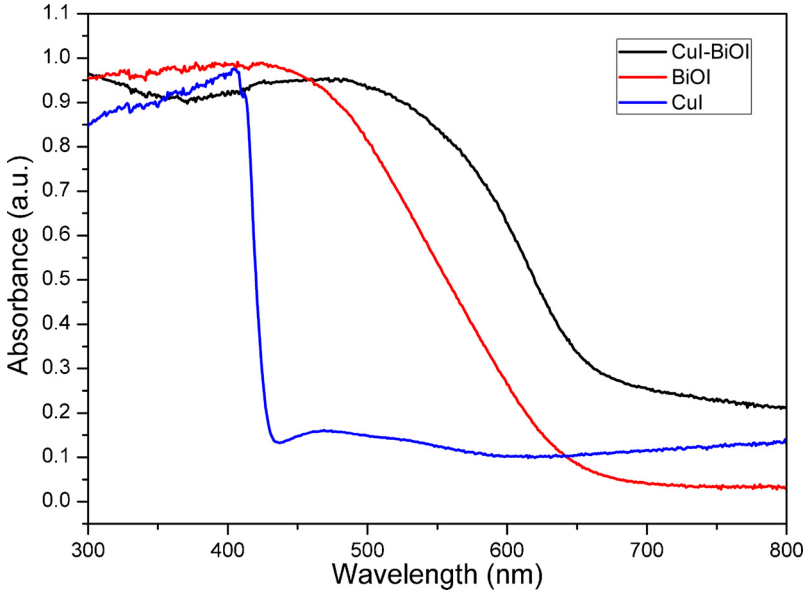


**Fig. 4.** UV–vis spectra of CuI, BiOI and CuI-BiOI.

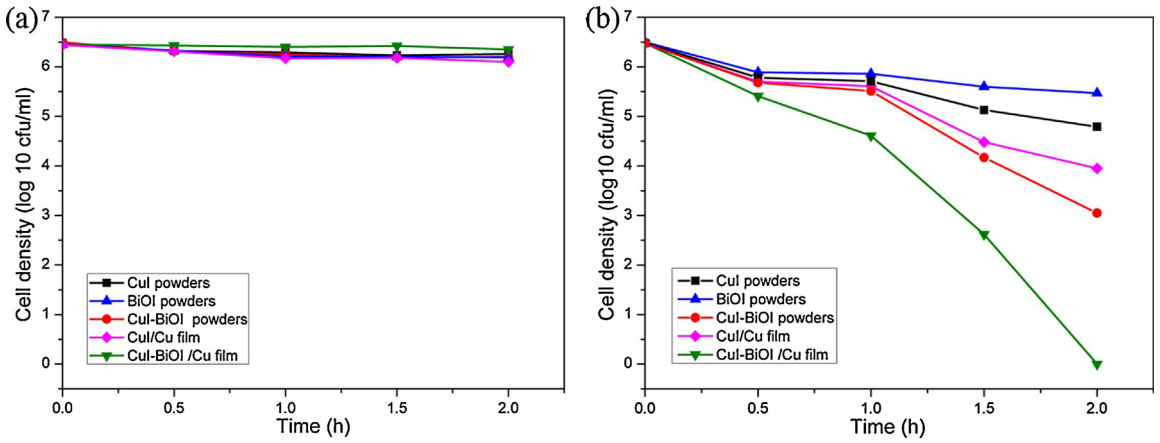


**Fig. 5.** *E. coli* K – 12 ($10^{6.5}$ cfu/mL) inactivation by prepared photocatalysts; (a) in the dark and (b) under visible light irradiation (≥ 400 nm).

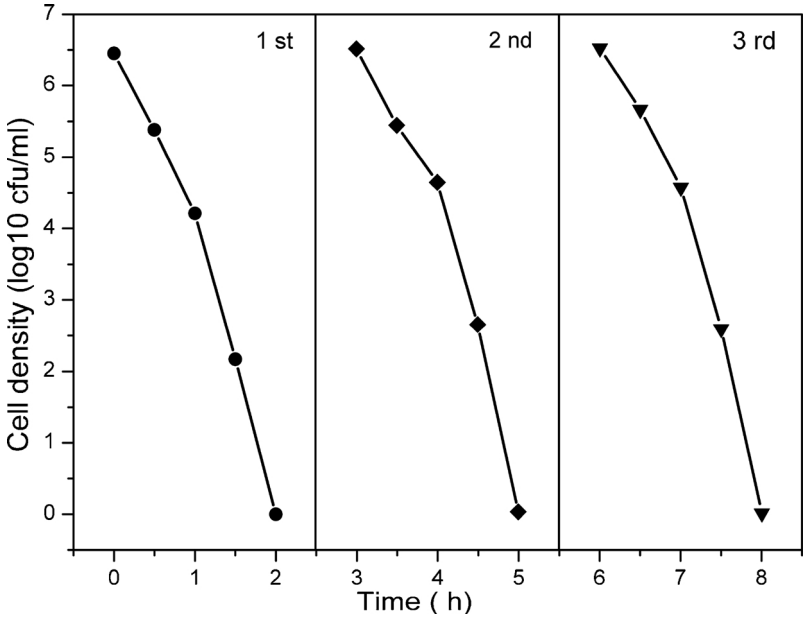


**Fig. 6.** Three cycling experiment in the disinfection performance with CuI-BiOI/Cu film under visible light irradiation.

However, for CuI-BiOI, the quantity of viable bacteria was approximately $10^{2.9}$ after visible light illumiation for 2 h, suggesting that the photocatalytic antibacterial activity of CuI-BiOI have been enhanced greatly than that of pure BiOI or CuI. Furthermore, when CuI-BiOI/Cu film was test under the same condition, all of the bacteria were disinfected after 2 h of visible-light irradiation, which indicates that copper sheet not only act as base material for supporting CuI-BiOI film but also improve the photocatalytic activity.

The photocatalytic stability of the CuI-BiOI/Cu film was investigated by three cycling experiment. The durability of the CuI-BiOI/Cu film composite were evaluated through the recycle of the used catalyst. For each cycle, the CuI-BiOI/Cu film was washed by deionized water. The results are shown in Fig. 6, negligible loss of activity could be observed after three successive cycle experiment. In addition, the XRD and XPS image of samples before and after reaction were given in Fig. S2 and S3 respectively. Obviously, there was no significant difference could be observed. Therefore, it is suggested that the CuI-BiOI/Cu film exhibit good stability for photocatalytic disinfection.

### 3.3. The mechanism of synergistic photocatalytic disinfection

According to the previous research of our group [22], the disinfection system of *E. coli* involved the generation of the reactive radicals such as ·OH, $\cdot O_2^-$, $H_2O_2$, $e^-$ and $h^+$ and the attack of reactive radicals to bacterial cells that may cause the decomposition of the cell walls. To identify the destruction process of normal bacterial cells in the CuI-BiOI photocatalytic system under visible light irradiation, the changes of microstructure and morphology of *E. coli* at different time intervals were examined by Laser Scanning Confocal Microscopy (LSCM). As shown in Fig. 7a, before irradiation, the cells of *E. coil* showed intact wall normally and exhibited rod-shaped morphology. After E. coil contact with CuI-BiOI under illumination for 1 h (Fig. 7b), some of bacterial structures were destroyed and clustered together. Part of their cells wall slightly appeared depression (red circle in Fig.7b). After 2 h of irradiation (Fig. 7c), the cells were extremely deformed and all of bacterial were gathered together. Ultimately, the *E. coli* were completely killed. According to reports [3], once the cell walls were disrupted, the cell content would leak out into the solution and the UV absorption can be used to demonstrate the protein of bacterial cell contents after cell disruption. The UV absorption at 280 nm was ascribed to the protein of *E. coli*, and the higher in the intensity of UV absorption, the higher concentration of cell contents in the solution. The human serum albumin (HAS) was used as a standard protein to calibrate unknown proteins, then the HAS solution with different concentration gradient was prepared for UV absorption. The standard protein curve was shown in Fig. S1 [24]. As shown in Fig. 8, with the

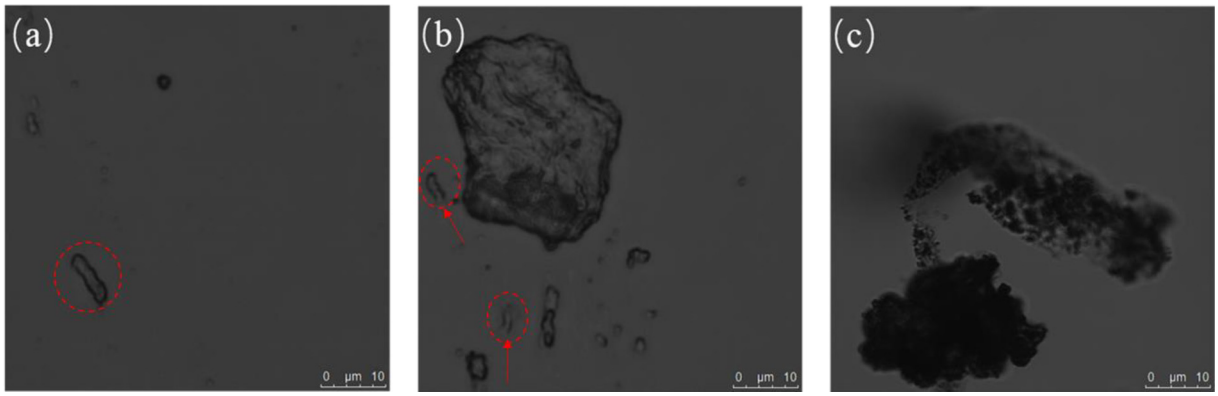


**Fig. 7.** LSCM images of *E. coli* ($10^{6.5}$ cfu/mL) photocatalytically treated with CuI-BiOI/Cu film under visible light irradiation for (a) 0 h, (c) 1 h and (d) 2 h. The red circles indicate the deformation, pore-forming, and fracture of *E. coli* (For interpretation of the references to colour in this figure legend, the reader is referred to the web version of this article).

increase of illumination time, the concentration of protein in bacterial solution increased gradually. These results suggested that the cell leakage in the solution increased gradually which were in good accordance with the change of bacterial LSCM images.

The cell leakage of bacteria was caused by the reactive radicals that can directly contact with bacterial cells and be responsible for photocatalytic bacterial inactivation [25]. However, which of these reactive radicals (·OH, $\cdot O_2^-$, $H_2O_2$, $e^-$ and $h^+$) plays the most important role in the photocatalytic sterilization process remains unclear and was quite different from various photocatalytic systems [22,26–28]. Hence, to gain an in-depth understanding of the individual role of ROS in the CuI-BiOI photocatalytic system, a series of experiments were carried out to investigate the exact roles of these reactive oxidative species by using particular scavengers to eliminate the corresponding reactive species (· OH, $\cdot O_2^-$, $H_2O_2$, $e^-$ and $h^+$). The scavengers used in this study were isopropanol for ·OH [29,30], TEMPOL for $\cdot O_2^-$ [31], Fe(II)-EDTA for $H_2O_2$ [28,32], Cr(VI) for electron ($e^-$) [29,33], and sodium oxalate for hole ($h^+$) [28,34], respectively. Before experiment, the applied concentration of each scavengers were optimized to ensure their best scavenging effect as well as to cause no cell inactivation [25]. As can be seen in Fig. 9, the addition of isopropanol and TEMPOL has less effects on the disinfection efficiency, indicating that ·OH and $\cdot O_2^-$ were not the main reactive species in this inactivation process. When Fe (II)–EDTA was added into the disinfection system, the quantity of viable bacteria was approximately $10^{2.3}$ after 2 h light irradiation that was higher than that of adding isopropanol and TEMPOL. However, when Cr(VI) or sodium oxalate was added into the disinfection system, the quantity of viable bacteria was approximately $10^{3.5}$ and $10^{3.8}$, respectively, suggesting that the Cr(VI) and sodium oxalate have great inhibition effect on the disinfection efficiency. These results indicate that the effect of reactive oxidative species on the antibacterial activity decreases in order $h^+ > e^- > H_2O_2 > \cdot HO > \cdot O_2^-$. This order is reasonable because photo-generated $h^+$ and $e^-$ for one hand could directly attack the bacteria that cause the death of bacterial. For the second hand, $h^+$ and $e^-$ generate other reactive oxidative species, such as $\cdot O_2$- that was product by $e^-$ reacting with $O_2$, ·OH and $H_2O_2$ that resulted from $h^+$ reacting with $OH^-$ in the water. These reactive oxidative species could further oxidize the cell wall and outer membrane of the bacteria. Thus, it is the efficient separation of $h^+$ and e- that plays the significant role in the photocatalytic inactivation of *E. coli*.

In this work, the CuI-BiOI/Cu film showed the best photocatalytic antibacterial activity than BiOI, CuI, CuI-BiOI and CuI/Cu film (Fig. 5b). The main reason may be ascribed to higher efficient separation of $h^+$ and $e^-$ on CuI-BiOI/Cu. To compare the separation of $h^+$ and $e^-$ among BiOI, CuI-BiOI powders and CuI-BiOI/Cu film, the photocurrent response which is a useful method to evaluate the charge

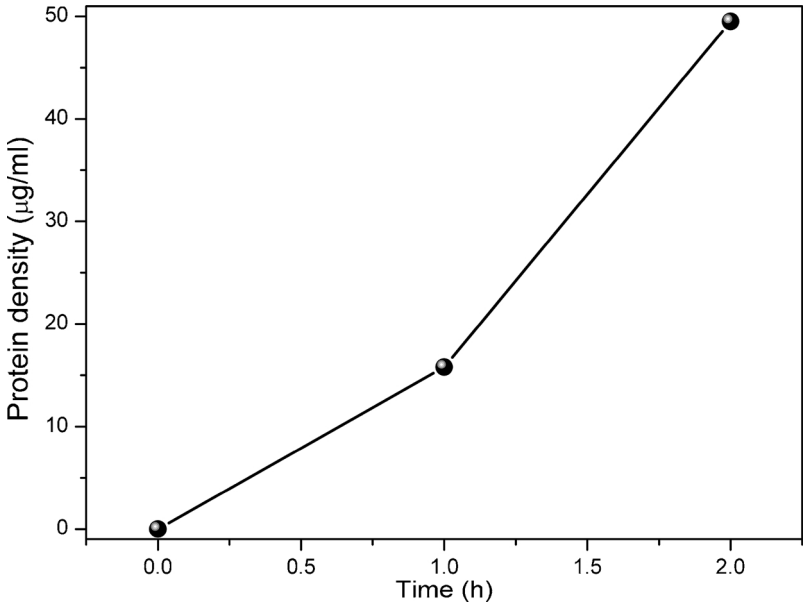


**Fig. 8.** The concentration of protein in bacterial solution of the photo-treated bacteria at different irradiation time intervals (0, 1 and 2 h).

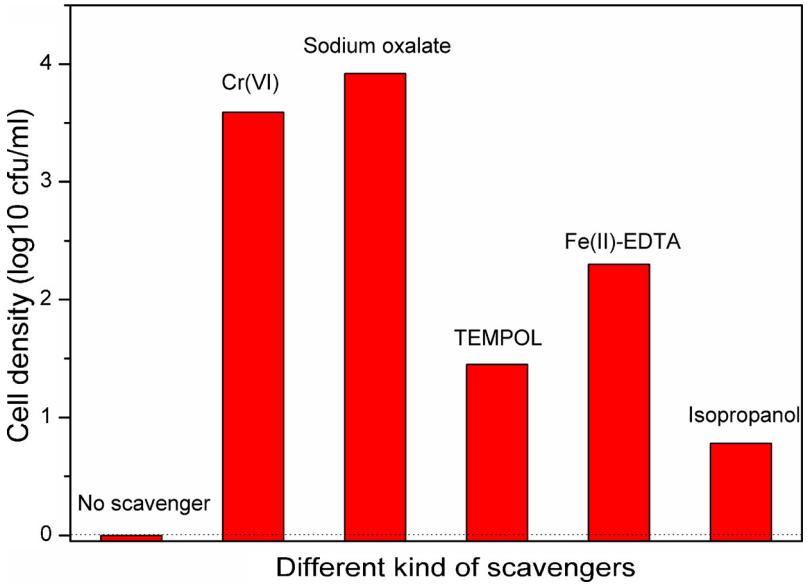


**Fig. 9.** Photocatalytic inactivation efficiency against *E. coli* K-12 ($10^{6.5}$ cfu/mL) with different scavengers (0.5 mM sodium oxalate, 0.5 mM isopropanol, 0.05 mM Cr (VI), 2 mM TEMPOL and 0.1 mM Fe(II)–EDTA) in the presence of CuI-BiOI/Cu film under visible light irradiation.

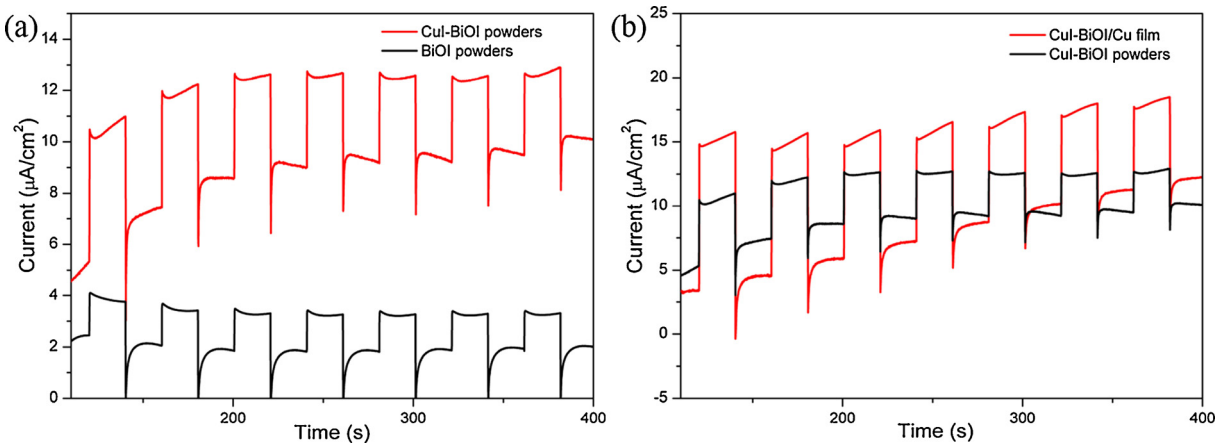


**Fig. 10.** Transient photocurrent responses prepared samples under visible light irradiation. (a) CuI-BiOI and BiOI powders, (b) CuI-BiOI powders and CuI-BiOI/Cu film.

separation were test. As shown in Fig. 10a, the photocurrent density generated by CuI-BiOI powders was much higher than that of pure BiOI. As displayed in Fig. S4, the electrochemical impedance spectroscopy (EIS) shows that the diameter of the semicircle arc of CuI-BiOI is the smaller than BiOI, indicating that the introduction of CuI contribute to enhanced charge transfer. As shown in Fig. S5a, the cyclic voltammograms (CV) shows the anodic and cathodic peaks of the reversible redox couple of $Fe(CN)_6^{4-}/Fe(CN)_6^{3-}$. Obviously, CuI-BiOI displayed the better redox peak current density than BiOI. These results suggest an improvement of the charge transfer efficiency in CuI-BiOI. The linear sweep voltammetry (LSV) in Fig. S5b indicate the same tendency of charge transfer enhancement. The results together demonstrate the more efficient charge transfer achieved within the samples by a sequence of CuI-BiOI > BiOI, which indicated that the introduced CuI can remarkably promote charge separation and enhance the photocatalytic performance of BiOI. In addition, after CuI-BiOI was coated on Cu sheet (as shown in Fig. 10b), the photocurrent density generated by CuI-BiOI/Cu film was much higher than that CuI-BiOI powders, suggesting that the Cu plays another critical role in charge separation. Base on the above results, the mechanism of synergistic photocatalytic bacterial inactivation was proposed in Fig. 11. The VB of CuI and BiOI is around 0.6 and 2.46 V versus normal hydrogen electrode (NHE) [35,36]. Under visible light irradiation, BiOI was excited and generated $h^+$ and $e^-$. The $e^-$ easily transfer to the *E. coli* solution through copper sheet, which promotes the separation of electron-hole pairs. The transferred $e^-$ not only directly attack the bacteria but also react with $O_2$ in the water and generate $\cdot O_2$. At the same time, the $h^+$ on the VB of BiOI spontaneously transferred to the VB of CuI and was trapped by the $H_2O$ and generated $\cdot OH$, $H_2O_2$ and $\cdot HO_2$. These oxidizing reactive species in the system could attack the bacterial cells, oxidize and disrupt the cell membrane, and finally lead to the death of the bacteria.

## 4. Conclusions

The CuI-BiOI/Cu film was successfully achieved by water bath method. Compare to pure BiOI and CuI, the prepared CuI-BiOI/Cu film showed considerable efficiency in photocatalytically inactivating E.

coli K-12 under VL irradiation. After 2 h visible light irradiation, almost all of the bacteria could be killed. The CuI act as a hole-transport channel for CuI-BiOI, and the copper sheet plays another critical role in electron transfer, which suppress the recombination of electron-hole pairs and result in higher photocatalytic antibacterial activity. This new synthetic strategy would provide us a new route for use of the photoactive functional film materials for water treatment field.

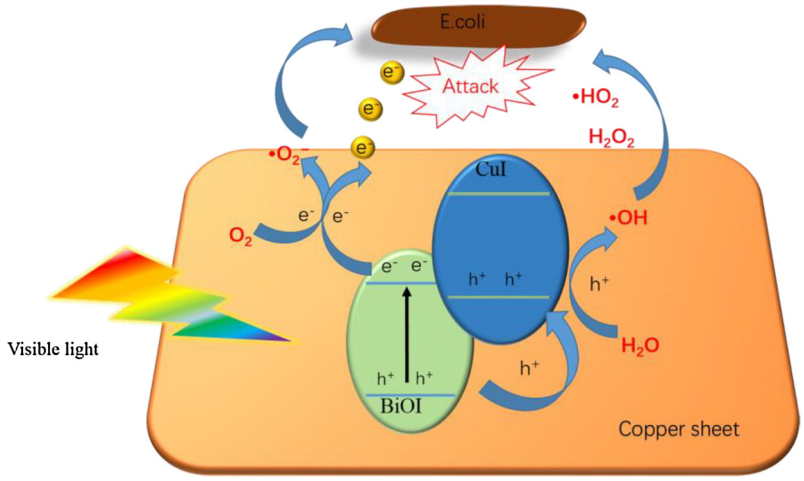


**Fig. 11.** Schematic drawing of the photocatalytic antibacterial process of CuI-BiOI/Cu film.

## Acknowledgement

This work was financially supported by NSFC (Nos. 21673042, 21673043 and 21773031).

## Appendix A. Supplementary data

Supplementary material related to this article can be found, in the online version, at doi:https://doi.org/10.1016/j.apcatb.2018.05.001.

## References

[1] R.P. Schwarzenbach, B.I. Escher, K. Fenner, T.B. Hofstetter, C.A. Johnson, U. von Gunten, B. Wehrli, Science 313 (2006) 1072.
[2] M.A. Shannon, P.W. Bohn, M. Elimelech, J.G. Georgiadis, B.J. Marinas, A.M. Mayes, Nature 452 (2008) 301–310.
[3] Y. Jia, S. Zhan, S. Ma, Q. Zhou, ACS Appl. Mater. Interfaces 8 (2016) 6841–6851.
[4] H. Lin, W. Deng, T. Zhou, S. Ning, J. Long, X. Wang, Appl. Catal. B: Environ. 176 (2015) 36–43.
[5] C. Liu, D. Kong, P.C. Hsu, H. Yuan, H.W. Lee, Y. Liu, H. Wang, S. Wang, K. Yan, D. Lin, Nat. Nanotechnol. 11 (2016) 1098.
[6] Y. Wang, Y. Long, D. Zhang, ACS Sustainable Chem. Eng. 5 (2017) 2454–2462.
[7] A. Henríquez, H.D. Mansilla, A.M. Martínez-de la Cruz, J. Freer, D. Contreras, Appl. Catal. B: Environ. 206 (2017) 252–262.
[8] Y. Cong, Y. Ji, Y. Ge, H. Jin, Y. Zhang, Q. Wang, Chem. Eng. J. 307 (2017) 572–582.
[9] J. Jiang, X. Zhang, P. Sun, L. Zhang, J. Phys. Chem. C 115 (2011) 20555–20564.
[10] L. Ye, J. Chen, L. Tian, J. Liu, T. Peng, K. Deng, L. Zan, Appl. Catal. B: Environ. 130 (2013) 1–7.
[11] H. Cheng, B. Huang, Y. Dai, Nanoscale 6 (2014) 2009–2026.
[12] X. Xiao, W.-D. Zhang, J. Mater. Chem. 20 (2010) 5866–5870.
[13] M. Sun, J. Hu, C. Zhai, M. Zhu, J. Pan, ACS Appl. Mater. Interfaces 9 (2017) 13223–13230.
[14] H. Wang, Y. Cai, J. Zhou, J. Fang, Y. Yang, Appl. Surf. Sci. 402 (2017) 31–40.
[15] X. Wang, Y. Shen, A. Xie, L. Qiu, S. Li, Y. Wang, J. Mater. Chem. 21 (2011) 9641–9646.
[16] Y. Zhou, M. lü, G. Zhou, S. Wang, S. Wang, Mater. Lett. 60 (2006) 2184–2186.
[17] X. Wang, J. Zhang, K. Zhang, W. Zou, S. Chen, RSC Adv. 6 (2016) 44851–44858.
[18] G. Dai, J. Yu, G. Liu, J. Phys. Chem. C 115 (2011) 7339–7346.
[19] L. Ye, L. Tian, T. Peng, L. Zan, J. Mater. Chem. 21 (2011) 12479–12484.
[20] P. Liu, E.J.M. Hensen, J. Am. Chem. Soc. 135 (2013) 14032–14035.
[21] I. Platzman, R. Brener, H. Haick, R. Tannenbaum, J. Phys. Chem. C 112 (2008) 1101–1108.
[22] S. Ning, H. Lin, Y. Tong, X. Zhang, Q. Lin, Y. Zhang, J. Long, X. Wang, Appl. Catal. B: Environ. 204 (2017) 1–10.
[23] M. Gao, D. Zhang, X. Pu, H. Ma, C. Su, X. Gao, J. Dou, Sep. Purif. Technol. 170 (2016) 183–189.
[24] A. Aitken, M.P. Learmonth, J.M. Walker (Ed.), The Protein Protocols Handbook, Humana Press, Totowa, NJ, 2009, pp. 3–6.
[25] W. Wang, L. Zhang, T. An, G. Li, H.-Y. Yip, P.-K. Wong, Appl. Catal. B: Environ. 108 (2011) 108–116.
[26] W. Wang, T.W. Ng, W.K. Ho, J. Huang, S. Liang, T. An, G. Li, J.C. Yu, P.K. Wong, Appl. Catal. B: Environ. 129 (2013) 482–490.
[27] W. Wang, Y. Yu, T. An, G. Li, H.Y. Yip, J.C. Yu, P.K. Wong, Environ. Sci. Technol. 46 (2012) 4599–4606.
[28] L.-S. Zhang, K.-H. Wong, H.-Y. Yip, C. Hu, J.C. Yu, C.-Y. Chan, P.-K. Wong, Environ. Sci. Technol. 44 (2010) 1392–1398.
[29] Y. Chen, S. Yang, K. Wang, L. Lou, J. Photochem. Photobiol. A Chem. 172 (2005) 47–54.
[30] A. Amine-Khodja, A. Boulkamh, C. Richard, Appl. Catal. B: Environ. 59 (2005) 147–154.
[31] D. Lejeune, M. Hasanuzzaman, A. Pitcock, J. Francis, I. Sehgal, Mol. Cancer 5 (2006) 21.
[32] Y. Chen, A. Lu, Y. Li, L. Zhang, H.Y. Yip, H. Zhao, T. An, P.-K. Wong, Environ. Sci. Technol. 45 (2011) 5689–5695.
[33] S.G. Schrank, H.J. José, R.F.P.M. Moreira, J. Photochem. Photobiol. A Chem. 147 (2002) 71–76.
[34] R. Jin, W. Gao, J. Chen, H. Zeng, F. Zhang, Z. Liu, N. Guan, J. Photochem. Photobiol. A Chem. 162 (2004) 585–590.
[35] Q. Wang, X. Shi, E. Liu, J.C. Crittenden, X. Ma, Y. Zhang, Y. Cong, J. Hazard. Mater. 317 (2016) 8–16.
[36] K. Tennakone, G.R.R.A. Kumara, I.R.M. Kottegoda, K.G.U. Wijayantha, V.P.S. Perera, J. Phys. D Appl. Phys. 31 (1998) 1492.